DMD Fast Forward. Published on November 7, 2019 as DOI: 10.1124/dmd.119.089151
This article has not been copyedited and formatted. The final version may differ from this version.

Title page

Title:

Assessment and Confirmation of Species Difference in Nonlinear Pharmacokinetics of Atipamezole with Physiologically Based Pharmacokinetic Modeling

Authors:

Zheng Li[a], You Gao [a], Chunmiao Yang [a], Yanan Xiang [a], Wenpeng Zhang[a], Tianhong Zhang[a], Ruibin Su [a], Chuang Lu[b], and Xiaomei Zhuang[*a]

Afflictions:

[a] State Key Laboratory of Toxicology and Medical Countermeasures, Beijing Institute of Pharmacology and Toxicology, Beijing, China

[b] Department of DMPK, Sanofi Company, MA, USA

Running Title Page

Running title: Nonlinear PBPK modeling of atipamezole

Corresponding Author:

Xiaomei Zhuang

State Key Laboratory of Toxicology and Medical Countermeasures

Beijing Institute of Pharmacology and Toxicology

Beijing

100850

China

Tel: +86 13683600728

Fax: +86 010 68211656

E-mail: xiaomeizhuang@163.com

Number of text pages: 16

Number of tables: 7

Number of figures: 9

Number of references: 40

Words in abstract: 249

Words in introduction: 716

Words in discussion: 1275

Nonstandard abbreviations:

AUC, area under the concentration-time curve; P450, Cytochrome P450; UGT,

UDP-glucuronosyltransferase; NADPH, β-nicotinamide adenine dinucleotide phosphate, reduced; UDPGA, uridine diphosphate glucuronic acid; FIH: first in human; PBS: phosphate buffer solution; LC-MS/MS, liquid chromatography tandem mass spectrometry; PK, pharmacokinetics; RLM, rat liver microsomes; HLM, human liver microsomes; IS, internal standard.

DMD Fast Forward. Published on November 7, 2019 as DOI: 10.1124/dmd.119.089151
This article has not been copyedited and formatted. The final version may differ from this version.

Abstract

Atipamezole, an α_2-adrenoceptor antagonist, displayed nonlinear pharmacokinetics (PK) in rats. The aim of this study was to understand the underlying mechanisms of nonlinear PK in rats and linear PK in humans and develop physiologically based PK models (PBPK) to capture and validate this phenomenon. *In vitro* and *in vivo* data were generated to show that metabolism is the main clearance pathway of atipamezole and species differences exists. Where CYP was responsible for the metabolism in rats with a low K_m, human specific UGT2B10 and 1A4 mediated N-glucuronidation was identified as the leading contributor to metabolism in humans with a high V_{max} capacity. Saturation of metabolism was observed in rats at pharmacological relevant doses but not in humans at clinically relevant doses. PBPK models were developed using GastroPlus™ software to predict the pharmacokinetic profile of atipamezole in rats after intravenous or intramuscular administration of 0.1-3 mg/kg doses. The model predicted the nonlinear PK of atipamezole in rats and predicted observed exposures within two-fold across dose levels. Under the same model structure, a human PBPK model was developed using human *in vitro* metabolism data. The PBPK model well described human concentration-time profiles at 10-100 mg doses showing dose proportional increases in exposure. This study demonstrated that PBPK is a useful tool to predict human PK when interspecies extrapolation is not applicable. The nonlinear PK in rat and linear PK in human were characterized *in vitro* and allowed the prospective human PK via *i.m.* dosing to be predicted at the preclinical stage.

Significance Statement

This study demonstrated that PBPK is a useful tool for predicting human PK when interspecies extrapolation is not applicable due to species unique metabolism. Atipamezole, for example, is metabolized by CYP in rats and by N-glucuronidation in humans that were hypothesized to be the underlying reasons for a nonlinear PK in rats and linear PK in humans. This was testified by PBPK simulation in this study.

Introduction

Nonlinear pharmacokinetic (PK) profiles are observed in preclinical studies in part because a wide dose range is studied. This sort of nonlinearity makes assessment of the relationships of dose-toxicity and dose-efficacy difficult due to the occurrence of non-dose-proportional exposure increase or decrease. It is therefore very crucial to qualitatively elucidate the underlying mechanisms and quantitatively predict nonlinear PK of a new chemical entity in humans (Fukuchi et al., 2007).

Atipamezole (Fig. 1) is a novel, potent and selective α_2-adrenoceptor antagonist devoid of significant interactions with other neurotransmitter receptors. It can rapidly reverse sedation anesthesia induced by α_2-adrenoceptor agonists. Hence, in veterinary practice, atipamezole has been commonly used to recover animals from sedation-anesthesia induced by α_2-adrenoceptor agonists for over two decades (Ewing et al., 1993). Animal studies suggest atipamezole enhanced sexual activity in rats and monkeys (Viitamaa et al., 1995; Pertovaara et al., 2004) and improved behavioral performance of rats subjected to focal cerebral ischemia (Puurunen et al., 2001; Pertovaara et al., 2005). Studies also suggested that atipamezole might have beneficial effects in the recovery from brain damage and might potentiate the anti-Parkinsonian effects of dopaminergic drugs (Pitkänen et al., 2004).

Atipamezole is currently being investigated for human application, however, a clear understanding of its disposition is lacking in both animals and humans.

Atipamezole has a high clearance and subject to significant first-pass clearance (Pertovaara et al., 2005), hence, intravascular (*i.v.*) and intramuscular (*i.m.*) routes are

considered as potential drug administration routes.

In the literature, human pharmacokinetics of atipamezole was characterized in a clinical study via single ascending *i.v.* administration at doses of 10-100 mg (Karhuvaara et al., 1990). Our preclinical characterization of atipamezole pharmacokinetics showed nonlinear PK in rats, yet linear increases in exposure were reported for human at a comparable exposure compared to rats (AUC range ~100 -4000 h×ng/ml). When single *i.v.* administration of atipamezole were given to rats from 0.3 to 3 mg/kg, the systemic plasma clearance of atipamezole decreased with increased dose. Therefore, there was a need to understand the underlying disposition of atipamezole in rats and humans and particularly the nonlinearity to better estimate pharmacokinetic and pharmacodynamics relationship and further build confidence around safety margins and dose escalation scheme for clinical trials with various administration routes (Bachmann and Belloto, 1999; Tachibana et al., 2012; Chirehwa et al., 2015; Wu et al., 2014).

Besides *in vitro-in vivo* extrapolation, traditional approaches for interspecies PK extrapolation is based on allometric scaling, which is an empirical prediction from animals to obtain human PK parameters (e.g., clearance, volume of distribution, Tang and Mayersohn, 2006). Those methods can be applied only to drugs with linear PK and no species unique metabolism exits for a given drug. For predicting and understanding saturable PK of a new drug candidate, mechanistic modeling and simulation approaches across species are increasingly being applied (Huang and Rowland, 2012; Shebley et al., 2018). Among the modeling and simulation

approaches, physiologically based pharmacokinetic (PBPK) model is a powerful tool to quantitatively delineate how certain extrinsic and intrinsic factors might influence the non-proportional systemic exposures. PBPK modeling is based on drug-dependent physicochemical and pharmacokinetic parameters as well as drug-independent physiological systemic parameters to capture the kinetics and dynamics of drug absorption, distribution, metabolism and excretion (ADME) (Rowland et al., 2011; Liu et al., 2013; Jones et al., 2015; Zhuang and Lu, 2016; Li et al., 2018). With broad application of PBPK modeling and many successful examples of predicting human PK and DDI, it is particularly useful in capturing linear and nonlinear processes simultaneously (Dong et al., 2011; Chen et al., 2013).

The purpose of this study is to utilize a PBPK modeling approach to predict both rat and human PK and predict exposures in humans after various routes of administration. To achieve this, key *in vitro* and *in vivo* data for atipamezole were generated in rats (*in vitro* and *in vivo*) and in humans (*in vitro* only) to understand the respective metabolism mechanisms and tissue partitioning. Then a bottom-up combined with top-down PBPK model was developed and applied in the assessment of nonlinear PK in rats and identifying the mechanism that led to the nonlinearity. Ultimately, a PBPK model was built to predict human PK using all available information from preclinical *in vitro* and *in vivo* studies, as well as the learnings from the rat PBPK model.

Materials & Methods

Chemical and reagents. Atipamezole hydrochloride was supplied by chemical synthesis laboratory of our Institute (Beijing, China) with purity greater than 99% (Supplemental Figure 1 is the NMR spectrum; Li et al., 2019). Midazolam (MDZ), 1'-OH-MDZ, phenacetin, acetaminophen, diclofenac, S-mephenytoin, 4-OH-diclofenac, 4-OH-mephenytoin, bupropion, OH-bupropion, amodiaquine, N-desethylamodiaquine, dextromethorphan, dextrorphan were all purchased from Sigma-Aldrich (St. Louis, MO). Human liver microsomes (150-donor pool, mixed sex), male rat liver microsomes, and recombinant UGT Supersomes (UGT1A1, 1A3, 1A4, 1A6, 1A8, 1A9, 2B4, 2B7, 2B10, 2B15, and 2B17) were purchased from Corning Life Sciences (Tewksbury, MA). NADPH was purchased from Roche Life Science (Basel-Stadt, Switzerland). Other reagents were of HPLC grade or better.

NADPH- and UDPGA-dependent hepatic clearance in liver microsomes. The CYP-mediated metabolic stability was conducted in incubations containing 1 μM of atipamezole in rat or pooled human liver microsomes (0.5 mg/ml) in 100 mM of potassium phosphate buffer with 5 mM of $MgCl_2$, pH 7.4. The mixture was pre-incubated at 37 °C for 5 min. NADPH (final concentration of 1 mM) was added to initiate the reactions. For UGT-mediated metabolic clearance assays, alamethicin at final concentration of 25 μg/mg protein, 1 μM of atipamezole and rat or human liver microsomes in 100 mM of potassium phosphate buffer (pH 7.4) were mixed on ice for 15 min. The mixture was then pre-incubated at 37 °C for 5 min. UDPGA (final concentration of 2.5 mM) was added to initiate the reactions. For combined NADPH and UDPGA mediated metabolism assays, the pooled liver microsomes of rat or human and drug solutions were treated as described above for the

glucuronidation assay. The reactions were initiated by adding mixture of NADPH (1 mM) and UDPGA (2.5 mM), final concentrations. Aliquots of the incubation were removed at 0, 5, 15, and 30 min and diluted in 4× volume of chilled acetonitrile containing internal standard to stop the reactions. After centrifugation at 13000 g for 10 min, the supernatant was collected and stored at -20 °C until LC-MS/MS analysis. The *in vitro* $t_{1/2}$ in liver microsomal incubation was calculated from the semi-log plot of atipamezole concentration remaining *vs.* incubation time and intrinsic clearance (CL_{int}, ml/min/kg) was calculated as following:

$$CL_{int} = \frac{0.693}{in\ vitro\ t_{1/2}} \times \frac{ml\ incubation}{mg\ microsomes} \times \frac{45\ mg\ microsomes}{g\ liver} \times \frac{X\ g\ liver}{kg\ BW} \quad (1)$$

For rat and human, X values of 40 and 25.7 were used, respectively (Davies and Morris, 1993).

The conversion of CL_{int} to hepatic clearance CL_h by a well-stirred model is described previously (Houston. 1994):

$$CL_h = \frac{Q_h \times CL_{int}}{Q_h + CL_{int}} \quad (2)$$

Identification of UGTs involvement in metabolism of atipamezole. To identify the hepatic UGTs involved and understand the difference in metabolizing enzymes responsible for the metabolism of atipamezole in humans, recombinant UGT of UGT1A1, 1A3, 1A4, 1A6, 1A8, 1A9, 2B4, 2B7, 2B10, 2B15, and 2B17 were incubated (0.5 mg/ml protein with 1 μM atipamezole) in a similar way as HLM described above. The reaction product after incubation and protein precipitation was analyzed on LC-MS/MS for the formation of glucuronides.

Measurement of Michaelis constant (K_m) in RLM using substrate depletion

method. Due to the lack of authentic standards of atipamezole metabolites, the Michaelis constant (K_m) of atipamezole towards P450 mediated biotransformation in RLM was obtained using a substrate depletion approach (Obach and Reed-hagen, 2002, Nath and Atkins, 2006). Various concentrations of atipamezole (0.32, 0.63, 1.25, 2.5, 5, 10, 20 µM) and rat liver microsomes (0.5 mg/ml) in 100 mM of potassium phosphate buffer (pH 7.4) with 5 mM of $MgCl_2$ were preincubated at 37 °C for 5 min. NADPH (1 mM, final concentration) was added to initiate the reactions. Aliquots were removed from incubations with various initial atipamezole concentrations at 0, 2, 5, 10, 15, and 30 min time points. The reactions were terminated by diluting the aliquots in 4× volume of chilled acetonitrile containing internal standard. The samples were processed for analysis by mass spectrometry as stated below. The log transformed percentage remaining of atipamezole were plotted against each time point for each incubation group to obtain the substrate depletion rate constants (k_{dep}). K_m value was then determined from the inflection point of a plot of the k_{dep} values versus the initial atipamezole concentrations in a semi-log plot following Eq. 3:

$$k_{dep} = k_{dep([s]=0)} \times (1 - \frac{[s]}{[s]+K_m}) \quad (3)$$

where [S] is the substrate concentration, $k_{dep([S]=0)}$ represents the theoretical maximum substrate depletion rate constant at an infinitely low-substrate concentration, and K_m is the Michaelis constant.

Enzyme kinetic parameters for UGT-mediated metabolism in HLM. A metabolite profiling study indicated that atipamezole is mainly metabolized by UGT in HLM and generate a single N-glucuronidation metabolite. The enzyme kinetic parameters (K_m and V_{max}) of atipamezole in HLM were obtained by determining the

DMD Fast Forward. Published on November 7, 2019 as DOI: 10.1124/dmd.119.089151
This article has not been copyedited and formatted. The final version may differ from this version.

formation of the UGT-conjugation metabolite at different atipamezole concentrations. Similar procedure as described above for the HLM clearance assay was applied in a 5 min incubation with initial concentration of 0.32, 0.63, 1.25, 2.5, 5, 10, and 20 μM. The amount of UGT-conjugated metabolite formed (pmol/min/mg protein) was calculated in the reference of known amount of atipamezole disappearance as described by Eq.4:

$$\frac{d_M}{d_t} = \frac{v_{max} \times [s]}{K_m + [s]} \quad (4)$$

The data were analyzed with the nonlinear analysis to generate K_m and V_{max} values (Pharsight Corporation, USA).

Non-specific protein binding. The extent of protein binding of atipamezole to plasma and liver microsomes of rat and human, and major tissue homogenates of rat (liver, kidney, lung, brain, fat, spleen, heart, gonad, and muscle) were determined using a 48-well Rapid Equilibrium Dialysis device (Thermo Bioscience, Woburn, MA). All rat tissues were homogenized in 4x volume (*w/v*) of PBS (pH 7.4). Rat or human plasma was spiked with atipamezole at three concentrations (1, 3 and 10 μM). Rat or human liver microsomes (0.5 mg/ml protein) and other tissue homogenates were spiked with atipamezole at final concentration of 1 μM. Aliquots of 200 μl of the spiked biological matrices were loaded into the donor side of a dialysis apparatus and 350 μl of buffer was added to the receiving side. The apparatus was incubated in a shaking incubator at 37°C for 4h. After incubation, the samples from donor and receiving chambers were diluted in the same matrixes in the other chamber so the final matrix composition was the same. The resulting samples were precipitated in acetonitrile with IS. The atipamezole concentrations were determined by LC-MS/MS.

DMD Fast Forward. Published on November 7, 2019 as DOI: 10.1124/dmd.119.089151
This article has not been copyedited and formatted. The final version may differ from this version.

The unbound fraction of atipamezole in plasma or liver microsomes ($f_{u,x}$) was calculated as shown in Eq. 5, and unbound fraction in the tissue homogenate ($f_{u,t}$) was calculated according to Eq. 6.

$$f_{u,x} = Conc_{buffer\ chamber}/Conc_{plasma/liver\ microsomes\ chamber} \quad (5)$$

$$f_{u,t} = Conc_{buffer\ chamber}/Conc_{tissue\ homogenate\ chamber} \quad (6)$$

The measured unbound fractions would be higher when a tissue is homogenized and diluted in buffer, the unbound fractions in an undiluted tissues ($f_{u,tissue}$) were calculated using Eq. 7.

$$Undiluted\ f_{u,tissue} = \frac{1/D}{((1/f_{u,tissue\ homogenate}) - 1) + 1/D} \quad (7)$$

Where D represents the fold of dilution factor in tissue homogenates. The free fraction of plasma and undiluted tissue are used in tissue-to-plasma exposure ratio calculation (Kalvass and Maurer, 2002).

Blood to plasma partitioning. The blood/plasma concentration ratio (R_{bp}) of atipamezole was determined by incubating the compound with fresh whole blood from rats and humans. Atipamezole (final concentration1 µM) was added to whole blood and an equal volume of plasma isolated from the same blood which served as a control for the whole blood concentration. The spiked whole blood and plasma were incubated at 37°C for 1 h. After incubation, the blood was centrifuged at 2000×g for 10 min, and 50 µl aliquots of plasma were removed. All incubations were performed in triplicate. The concentrations of atipamezole in plasma separated from the blood and plasma spiked directly with atipamezole were determined by LC-MS/MS. R_{bp} was calculated by dividing the concentration in the plasma spiked directly with atipamezole by the concentration in the plasma separated from blood after incubation.

Disposition and tissue distribution of atipamezole in rats. Male SD rats (200 to 220 g) were obtained from Beijing Vital River Laboratory Animal Technology Co., Ltd. (Beijing, China). Animals were housed in a temperature and humidity-controlled room with a 12 h light/dark cycle. They were fasted 12 h prior the experiments and had ad libitum access to water. The animal experiments were conducted in the Beijing Center for Drug Safety Evaluation and according to a protocol approved by the Institutional Animal Care and Use Committee of the Center, which followed the guidelines of the Association for Assessment and Accreditation of Laboratory Animal Care International (AAALAC). The animal protocol number is IACUC-2017-053. For PK investigation, 36 rats were randomly divided into six groups (each group consisting of six rats). Three groups were given intravenous *(i.v.*) bolus injection of atipamezole solution via the tail vein at the doses of 0.3, 0.9, 3 mg/kg. The other three groups were given intramuscular (*i.m.*) injection of atipamezole solution at the doses of 0.1, 1, and 3 mg/kg. Atipamezole was formulated in saline. For all groups, at sampling times of 0, 0.033, 0.083, 0.25, 0.5, 1, 2, 4, 6, 8, 10, 12 and 14h after dosing, 0.2 ml blood samples were collected into heparinized polypropylene tubes. The plasma samples were collected after centrifugation of the blood samples at 2000×g for 10 min and stored at -20^{o}C until analysis using an established LC-MS/MS method.

For tissue distribution study, 24 male rats (6 animals for each time point) were dosed (*i.m.*) with the atipamezole solution at 1 mg/kg. The animals were anaesthetized and exsanguinated at 0.25, 1, 4, 24h post dose. After perfusion with

PBS via ventriculus sinister for 2 minutes, major tissues (liver, kidney, lung, brain, adipose, spleen, heart, gonad, and muscle) were harvested and rinsed with cold saline and blotted dry with filter paper. Tissue samples were homogenized and atipamezole quantitated along with plasma samples using the LC-MS/MS method. The tissue-to-plasma concentration ratios were calculated by dividing tissue concentration over plasma concentration at the indicated time (0.25, 1, 4, 24h post dose) and referred as the tissue-to-plasma partition coefficient (K_p).

Brain distribution at different dosage. 36 male rats were divided into 3 groups and dosed with the atipamezole solution at 0.3, 1 and 3 mg/kg *i.m.* Animals were anaesthetized and then exsanguinated at 0.25, 1, 4, 24h after dosing (3 animals for each time point). Plasma and brain were harvested and processed with the same methods described above for atipamezole concentration determination.

Sample process and analysis methods. Plasma, blood, microsomal, and tissue homogenates samples were precipitated with 4× volume of acetonitrile followed by centrifugation to remove protein. The acetonitrile contains propranolol (30 ng/ml) as internal standard (IS). The concentrations of atipamezole in all samples were determined by a reported LC-MS/MS method (Li et al., 2019) using an MRM positive mode with mass transition (*m/z*) of 213.1 to117.0. The method fulfilled with pre-set acceptance criteria (in-house analytical method validation protocol), including QC precision (RSD less than 15%), QC accuracy (85%-115%), stability (precision and bias less than ±15% for three cycles of freeze/thaw). Long team stability was tested at -20°C and -40°C for 4 weeks and short team stability was tested for 24 h at room

temperature. The calibration/standard curve linearity ranges 0.5-1000 ng/ml with correlation coefficient r^2 >0.99. The method met the acceptance criteria according to the bioanalytical method validation standard established by the FDA. The pharmacokinetic parameters for atipamezole were calculated by noncompartmental analysis using WinNonlin Phoenix v6.3 (Pharsight, Sunnyvale, CA).

Atipamezole GastroPlus™ PBPK model. A full PBPK model was constructed for atipamezole mainly using bottom-up and top-down approach (Jamei et al., 2009) in GastroPlus™ simulator (version 9.6). The work flow of the model construction, verification and prediction is presented in Fig. 2. PBPK model was initially developed for a simple pharmacokinetic profile of atipamezole in rats via *i.v.* route at low dose (0.3mg/kg) which only includes clearance and distribution processes. Key parameters (i.e., physicochemical parameters, R_{bp}, $f_{u,p}$, $f_{u,mic}$), K_m value generated from RLM incubation, V_{max} value back-calculated from *in vivo* clearance and measured K_p values of individual tissues were as input information are presented in Table 1 and Table 2. Then the nonlinear pharmacokinetic profiles of atipamezole in rats via *i.v.* administrative across ascending dosages were verified with observed data from rat PK studies. In the next step, the PBPK model was employed for rat *i.m.* pharmacokinetic by alternating the dosing route. After nonlinear PK behaviors of rat were successfully observed with both *i.v.* and *i.m.* dosing routes, this PBPK model was extrapolated to human using human specific parameters, i.e. *in vitro* enzyme kinetic data combined with tissue distribution profiles converted from K_p values obtained in rats corrected with plasma binding data (Table 2). Population-dependent

physiological parameters in the Population Estimates for Age-Related Physiology™ (PEAR) module of GastroPlus™ v9.7 were used in our human PBPK model. Customized information, such as age, gender, height, and body weight in a Caucasian population were set up to match the patient characterization in a published clinical trial which was used to verify our human model (Karhuvaara et al., 1990).

Statistical analysis. In *in vitro* study, replicated incubations/samples were performed (n=3), and all positive and negative control groups were included simultaneously. In i*n vivo* study, replicated animals/samples were performed (n=6). All measured data were presented as means ± standard deviation. For the comparison of measured K_p values of individual tissues and their predicted K_p values using the GastroPlus™ software (Table 2), ratio of two values beyond 0.5-2 is defined as significant difference. For accuracy assessment of a model simulation, acceptance is set to be within 2-fold. For comparison between groups, the statistically significant difference is set for a P value of less than 0.05 using analysis of variance, with the Student's t-test.

Results

***In vitro* metabolic stability of atipamezole.** Atipamezole was found to be metabolized in RLM and HLM to different extents in presence of co-factors of CYPs (NADPH) and/or UGTs (UDPGA). The percentages of atipamezole remaining at various time points are presented in Fig. 3. The turnover of atipamezole in RLM only occurred in the presence of NADPH, no decrease of parent drug concentration was observed in the presence of UDPGA. Co-incubation with both cofactors had similar depletion rate as the NADPH only (Fig. 3A). In HLM, the disappearance

rate of atipamezole is much greater in the presence of UDPGA than in the presence of NADPH. Co-incubation with both cofactors led to almost no increase in turnover rate as UDPGA alone suggested the direct glucuronidation was the major clearance pathway in HLM (Fig. 3B). The intrinsic clearance and extrapolated hepatic clearance of atipamezole were calculated from data presented in Fig. 3.

In RLM, the hepatic clearance of atipamezole driven by CYP was 31.7±0.8 ml/min/kg which was close to rat *in vivo* clearance (39.9±5.8 ml/min/kg, Table 5). Additionally, an earlier metabolism profiling study in rats detected little parent drug in urine and bile and circulating oxidized-metabolites were mainly presented in bile (data not presented). That confirmed hepatic metabolism is the major clearance pathway for atipamezole in rats catalyzed predominantly by P450.

In HLM, UGT-mediated hepatic clearance (19.4±0.02 ml/min/kg) played a more important role compared to that by CYP (9.7±1.8 ml/min/kg). With the presence of both NADPH and UDPGA, the hepatic clearance (19.3±0.04 ml/min/kg) is almost identical to that of only UDPGA presence as a cofactor (Table 3). UGT-mediated hepatic clearance is also close to the *in vivo* clearance of atipamezole reported in human (21.3±2.8 ml/min/kg) (Karhuvaaral et al., 1990), as well as to human hepatic liver blood flow (20.7 ml/min/kg) (Davis and Morris, 1993). These results demonstrated that hepatic metabolism is the leading elimination route of atipamezole in humans catalyzed primarily by UGT. The *in vitro* and *in vivo* metabolite identification has also been conducted in HLM and RLM with NADPH or UDPGA as cofactors and bile from BDC rat to testify the liver metabolism (Supplemental Figure

2-6, Li et al., 2018). Three oxidation metabolites were identified in RLM and HLM in the presence of NADPH. In the bile of BDC rat, the same three oxidation metabolites were excreted. Additionally, only a single UGT-conjugated metabolite was found in HLM with UDPGA.

Recombinant UGTs involved in human hepatic metabolism. Among 11 rUGTs tested, only UGT2B10 and 1A4 were identified to contribute to the hepatic metabolism of atipamezole. Based on equal molar incubations, rUGT2B10 played a more important role than rUGT1A4 at an approximately 15:1 ratio.

Michaelis constant of atipamezole in RLM and HLM. Two methods were utilized to estimate the Michaelis constant of atipamezole in RLM and HLM due to the different metabolizing enzyme involved in the biotransformation of atipamezole in in rats and humans and lack of metabolite standards. In RLM, the k_{dep} values at various initial concentrations were determined using a substrate depletion assay (Obach et al., 2002; Nath and Atkins 2006)). The plot of *in vitro* depletion rate constants versus substrate concentration for atipamezole in RLM is shown in Fig. 4A. The obtained total K_m value in RLM was 1.7±0.03 μM (361±6 ng/ml). The enzyme kinetic parameters of atipamezole in HLM were determined using the N-glucuronidation metabolite formation rate. The K_m and V_{max} values obtained from the Michaelis-Menten plot were 2.89±0.27 μM (614±57 ng/ml) and 1.07±0.03 nmol/min/mg protein, respectively (Fig. 4B).

Unbound fractions of atipamezole in plasma. Atipamezole was tested in rat and human plasma at 37 ºC for 4 hours and found to be stable (with recoveries of

96.7-113.8%). Unbound fractions of atipamezole in rat or human plasma were determined to identify the potential of protein binding effect on nonlinear PK. Our results showed no obvious species difference in the unbound fraction in plasma, the atipamezole free fraction was 0.085 for rats and 0.067 for humans. Moreover, the unbound fractions in rat or human plasma were concentration independent (Table 4).

Nonlinear PK behavior of atipamezole in rats. Mean atipamezole plasma concentration-time profiles in rats after various *i.v.* (A) and *i.m.* (B) doses are presented in Fig. 5. Existence of marked nonlinear pharmacokinetics at 3 mg/kg is manifested by the dose-normalized AUC profiles in both *i.v.* (C) and *i.m.* administrations (D). Pharmacokinetic parameters (Table 5) showed ~3-fold increase in dose (~1 to 3 mg/kg) resulted in 7.7 and 6.1-fold increase in AUC after *i.v.* and *i.m.* administration, respectively, indicating a super-proportional dose-exposure relationship. Total plasma clearance after intravenous dosing decreased notably when dose increased from 0.3 mg/kg to 3 mg/kg (i.e. from 39.96 ml/min/kg to 13.96 ml/min/kg). However, no obvious changes were observed in volume of distribution (*i.v.* route) and dose normalized C_{max} (*i.m.* route).

In vitro unbound K_m value of atipamezole in RLM is 137 ng/ml (0.65 μM) which is close to the unbound C_{max} (109 ng/ml) observed in rats after *i.m.* administration of 3 mg/kg of atipamezole. The unbound C_{max} was calculated from the total C_{max} of 1283 ng/ml with an average $f_{u,plasma}$ of 0.085 from the present study. The nonlinear PK may be attributed from the saturation of hepatic CYP metabolism in rats. In contrast, the *in vitro* unbound K_m value of atipamezole in HLM in the presence of NADPH and

DMD Fast Forward. Published on November 7, 2019 as DOI: 10.1124/dmd.119.089151
This article has not been copyedited and formatted. The final version may differ from this version.

UDPGA was 361 ng/ml (1.7 μM) which is much higher than the unbound C_{max} of 33 ng/ml (0.16 μM) reported in clinical trial at 100 mg QD dose (Karhuvaara et al., 1990).

Brain tissue distribution. Further investigation on potential factors contributed toward the nonlinear PK behavior was focused on the drug target tissue, i.e. brain to plasma ratios (K_p) at different doses, to investigate whether there is a target mediated drug disposition (TMDD). Disproportional increase of exposure in brain was observed as the fold of concentrations normalized to the low dose increased from 1-fold to 3.9 and 17.4-fold with dose increased from 0.3 to 1 and 3 mg/kg (observed and predicted AUCs are presented in Table 7), respectively. However, the $K_{p,uu}$ values stayed around 1.4-1.5 from 0.3 mg/kg to 3mg/kg suggesting a rapid equilibrium of atipamezole between brain and plasma and the nonlinear brain concentration is mainly driven by plasma concentration.

PBPK modeling in rats. PBPK model was established in rats with modules of passive diffusion and metabolic clearance using, 1) a back-calculated V_{max} from *in vivo* clearance and *in vitro* determined K_m, and 2) distribution parameters (K_p) determined from tissue distribution assays in various organs. Lukacova K_p (Miller et al., 2019) method was also used to predict the K_p values. The predicted and measured K_p values of individual tissues (Table 2) were found to be statistically deferent, i.e. measured and predicted value ratios were beyond 0.5-2 folds in most of the organs. This led us to use the measured tissue partitioning values instead of the predicted values. A comparison of PK profiles using either measured or predicted

K_p values are presented in Fig. 6, along with the observed PK from *in vivo* study. As one can tell, the PBPK simulation using predicted K_p values led to poor prediction of PK.

Fig. 7 showed the simulated intravenous plasma concentration-time profiles over different doses in rats that are well matched with the observed nonlinear PK profiles. This result demonstrates that the assumptions of permeability limited distribution and CYP mediated hepatic clearance were able to predict the nonlinearity observed in rats. This rat PBPK model was also able to predict the plasma concentration-time profiles over different doses after *i.m.* administration in rats. After *i.v.* administration, the ratios of AUC normalized to the lowest dose were 1: 3.3: 22 (predicted) and 1: 3.8: 30 (observed) for doses of 0.3, 0.9, 3 mg/kg, respectively. After *i.m.* administration, the corresponding ratios of AUC for predicted and observed were 1: 12.8: 56 and 1: 12.4: 75 from 0.1, 1, 3 mg/kg, respectively. Overall, the model achieved a good correlation coefficient between predicted and observed values with $r^2 > 0.86$, and the predicted plasma concentrations described by $AUC_{0\text{-inf}}$ were all within 0.89-1.41-fold of those observed values (Table 6).

PBPK prediction in humans and confirmation with clinical observation. The PBPK model for rat was initially applied to humans with the same mechanism, i.e. saturable metabolism to investigate whether nonlinear PK would be observed in humans. However, predicted human PK was linear in the clinically relevant doses (10-100 mg). In the investigation of metabolizing enzymes involved, *in vitro* studies highlighted that UGTs were mainly responsible for the metabolism of atipamezole in

humans which is different from that in rats.

In addition, liver clearance can be roughly expressed by UDPGA-mediated clearance. For distribution, K_p values from rats were calibrated using human $f_{u,plasma}$ to predict K_p in humans. This calibration was based on the observation that the predicted volume of distribution in rats is close to the actual observed value of distribution, and tissue distributions tend to have little species difference (Rowland et al., 2011). These assumptions were further confirmed by our human PBPK modeling, as the predicted plasma AUCs and volume of distribution were in good agreement with the available clinical data from three doses from the literature (Karhuvaara et al., 1990).

As mentioned above, besides using the transformed K_p values from rats, *in vitro* measured V_{max} and K_m in HLM in the present with NADPH and UDPGA and $f_{u,mic}$ were used in our model to define the overall clearance and metabolic pathways. The observed and predicted human PK profiles for each group are presented in Fig. 8 and Table 6. These data showed the predicted PK captured the reported PK quite well with about 155%-175% over prediction. A few factors may contribute to this deviation, such as the sparse clinical time points and the use of *in vitro* hepatic clearance as the whole-body clearance. For *i.m.* administration, the predicted human PK was conducted at projected efficacious doses of 10-100 mg as well as higher doses. The PK is proportional to the dose up to 1000 mg (Fig. 9) and then becomes greater than proportional above 1000 mg.

Considering atipamezole has no species differences in its receptor affinity for

α_2-adrenoceptor subtypes in humans and rodents (Haapalinna et al., 1997), brain exposure in rats under pharmacological efficacious dose (1 mg/kg, *i.m.*) is a practical way to bridge to human efficacious exposure. Table 7 summarized the PBPK model predicting brain exposure of atipamezole in rats and humans at different doses, along with the observed exposure from this study. Results showed AUC in human brain at 30 mg/person is close to that in rats at 1 mg/kg.

Discussion

When a drug candidate shows nonlinear PK in preclinical study, it can be a challenge to predict an appropriate efficacious dose for clinical trials. Special attention is also required when carrying out dose escalation during phase I clinical trials. Hence, it is important to understand the factors contributing to the nonlinear PK. Nonlinear PK is believed to be mainly associated with absorption, hepatic metabolism, protein binding, liver uptake, or target tissue distribution (Ludden, 1991; Han et al., 1999; Takeuchi et al., 2001). During the preclinical PK study of atipamezole in rats, AUC normalized by the dose (AUC/dose) was found to increase markedly beyond 500 $\times 10^{-6}$ h×kg/ml as the dose increased. This dose-dependent nonlinear exposure is within the efficacy regiment in rats (unpublished pharmacology study data in rats). Plasma protein binding was consistent across the rats and humans at different concentrations. The drug target site of atipamezole is mainly in CNS, and brain distribution could be an additional pathway of drug disposition/elimination (Smith et al., 2018). Our results show that although brain concentration was dose-dependent super-proportional increased, the $K_{p,uu}$ values was consistent across

doses, suggesting that brain free concentrations were driven by the plasma free concentrations, and in turn, the efficacy. To elucidate whether liver uptake is also involved in the saturable pharmacokinetics of atipamezole, transport experiments with LLC-PK1/MDR1 cells was carried out. The average $P_{app\ (a\text{-}b)}$ and $P_{app\ (b\text{-}a)}$ of atipamezole is $80.3\pm5.8\times10^{-6}$ and $88.0\pm8.4\times10^{-6}$ cm/s (Li et al., 2019), respectively, suggesting high permeability and passive transport of atipamezole across the bio-membrane to be a major mechanism, even if an active uptake might exist. On the other hand, although the K_p values of several tissues are far higher than 1, the $K_{p,uu}$ values were much lower than K_p values after corrected by f_u (K_p,uu in Table 2). Especially, with low value of the $K_{p,uu}$ of liver (0.06), together with high intrinsic clearance suggesting extensive metabolism occurred in liver and that attributes to low intracellular free drug concentration (Lu et al., 2006). Therefore, it suggested active uptake is unlikely to play a critical role in the mechanisms of the nonlinearity. However, it would be beneficial to further investigate this subject to clarify the possibility of involvement of carrier-mediated uptake, especially in humans. Mass balance study in rats showed a minimal parent recovery in feces and urine with less than 1% (0.28%). Metabolites of atipamezole were mainly detected in bile, suggesting the liver is the major elimination organ for atipamezole. Taken together, target site distribution has limited impact on the nonlinear PK of atipamezole, and saturation of metabolism seemed to be the main reason for nonlinear PK in rats.

In liver microsomes of rats and humans, significant difference in the hepatic clearance of atipamezole was identified. The clearance of atipamezole in rats was

driven by CYP enzymes, while UGTs played a major role for the clearance in HLM. Further phenotyping study in HLM showed UGT1A4 and UGT2B10, but not other UGT isoforms, were responsible for the N-glucuronidation of atipamezole, where UGT2B10 played a more significant role. UGT1A4 and UGT2B10 are known to specifically mediate N-glucuronidation, especially on tertiary amine, as the N-glucuronidation on primary and secondary amines tend to not be stable. These are human liver specific enzymes and do not present in rodents (Hawes 1998; Kaivosaari et al., 2011). Besides high abundance in humans, these enzymes are also present in dogs and monkeys with low abundance (Kaivosaari et al., 2008). UGT2B10 tends to have high affinity (K_m) and low capability (V_{max}) whereas UGT1A4 tends to have low affinity (K_m) and high capability (V_{max}), as reported in a study of two optical enantiomers of medetomidine: dexmedetomidine and levomedetomidine (Kaivosaari et al., 2008). We observed a similar kinetics for atipamezole with a low K_m in HLM as UGT2B10 played a major role. Because N-glucuronidation is a human-specific metabolic pathway and atipamezole contains tertiary amine, this explains the observed species difference in metabolism of atipamezole between rats and humans. PBPK modeling and simulation was taken as a powerful tool to capture the dose-exposure relationship of atipamezole for both rats and humans based on reasonable assumptions, while species difference in metabolism made IVIVE and allometric scaling impractical. Firstly, understanding clearance and distribution are essential for PBPK model construction. For atipamezole, identification of hepatic metabolism as the major elimination route enhanced confidence in defining and

inputting clearance in our PBPK models. In addition, metabolism-related nonlinearity is often influenced by the drug plasma concentrations as well as its kinetic parameters (K_m and V_{max}) for hepatic metabolism enzymes (Ludden, 1991). Determination of K_m, is usually assessed by the rate of metabolite formation against a series of substrate concentrations. However, authentic metabolites are required in this approach to quantify the formation of metabolite(s), which often are not available in drug discovery or even development stages. For atipamezole, due to multiple CYP-mediated oxidation, metabolites were identified in RLM incubation and standard metabolites were not available. As such, the parent disappearance half-life assay at different atipamezole concentrations to capture the saturation of metabolism phase was applied to determine the K_m in RLM (Obach and Reed-Hagen, 2002). A later publication provides a method to calculate the V_{max} from the same set of data (Nath and Atkins 2006). The V_{max} of atipamezole calculated from Nath and Atkins's method was within 2-fold of that back calculated from i*n vivo* clearance. In this study, the back calculated V_{max} of atipamezole with a middle-out approach was used in the PBPK modeling. In HLM, since glucuronidation metabolite was found to be the dominant metabolite in a metabolite profiling study, *in vitro* measured K_m and V_{max} values toward UGT-mediated N-glucuronidation of atipamezole were directly employed in the PBPK model by a bottom-up approach.

Understanding tissue distribution is also essential for PBPK modeling. In the present study, tissue distribution experiments in rats indicated atipamezole distributed rapidly to most tissues, including lung, liver, spleen, brain, adipose, kidney, heart, and

muscle, and their concentration-time profiles were parallel to the blood concentration-time curve. In the full PBPK distribution model, we therefore assumed that the drug distributes instantaneously and homogeneously within each tissue and that its uptake is limited by the blood flow (perfusion limited module in the GastroPlus^{TM}). Furthermore, in the current study, transporter-mediated tissue permeation and distribution for atipamezole were not considered based on a previous study that showed atipamezole is not a substrate of P-gp (Li et al., 2019). The tissue-to blood partitioning coefficients (K_p) were determined in rats and incorporated into the PBPK model with respective free fractions ($f_{u,t}$) for each individual tissue. Our results also show that using experimentally determined K_p values generated better PK prediction in PBPK modeling, although software prediction based on physicochemical properties has certain merit. The K_p values are believed to carry minimal species difference, thus in this study, converted human K_p values were calculated from the ratio of free concentration of atipamezole in human plasma over its free concentrations in rat tissues. The PBPK prediction using these converted K_p values showed a good PK prediction in humans. Although intramuscular administration is not a popular route in drug administration, it is still an effective route for first-aid administration and avoiding first-pass elimination. In the rat PBPK modeling of atipamezole via *i.m.* administration, selecting suspension formation in the software was found to provide a better prediction of PK profiles (e.g. T_{max} and C_{max}) over the solution formation. This might be attributed to the fact that administration of a drug in solution via *i.m.* route would have a similar delay in

absorption, as well as distribution in the body as if the drug was in suspension.

In summary, our study exemplifies that sometimes there is a "cross species barrier" for extrapolating animal PK to human PK. Understanding the species similarity or difference in metabolism/transport and sometimes excretion is important in the preclinical space for the prediction of PK or DDI risks in human. This study demonstrates a PBPK model that can capture nonlinear PK in rat with both *i.v.* and *i.m.* dosing routes. It provides insights into potential clinical application of atipamezole via *i.v.* or *i.m.* administration routes.

Acknowledgment

The authers greatly appreciate the help of Dr. Jennifer Fretland in editing this manuscript.

Authorship Contributions

Participated in research design: Zhuang, Li, Su, and Lu.

Conducted experiments: Li, Gao, Yang, Xiang, and Zhang.

Contributed new reagents or analytic tools: Su.

Performed data analysis: Zhuang, Li, and Zhang.

Wrote or contributed to the writing of the manuscript: Zhuang, Li, and Lu.

References:

Bachmann KA and Belloto Jr RJ (1999) Differential kinetics of phenytoin in elderly patients. *Drugs Aging* **15**:235-250.

Chen T, Mager DE, and Kagan L (2013) Interspecies modeling and prediction of human exenatide pharmacokinetics. *Pharm res* **30**:751-760.

Chirehwa MT, Rustomjee R and Mthiyane T (2015) Model-based evaluation of higher doses of rifampin using a semimechanistic model incorporating autoinduction and saturation of hepatic extraction. *Antimicrob Agents Chemother* **60**:487-494.

Davis B and Morris T (1993) Physiological parameters in laboratory animals and humans. *Pharm Res* **10**:1093-1095.

Dong JQ, Salinger DH, Endres CJ, Gibbs JP, Hsu CP, Stouch BJ, Hurh E, and Gibbs MA (2011) Quantitative prediction of human pharmacokinetics for monoclonal antibodies: retrospective analysis of monkey as a single species for first-in-human prediction. *Clin pharmacokinet* **50**:131-142.

Ewing KK, Mohammed HO, Scarlett JM and Short CE (1993) Reduction of isoflurane anesthetic requirement by medetomidine and its restoration by atipamezole in dogs. *Am J Vet Res* 5**4**:294-299.

Fukuchi Y, Toshimoto K, Mori T, Kakimoto K, Tobe Y, Sawada T, Asaumi R, Iwata T, Hashimoto Y, Nunoya K, Imawaka H, Miyauchi S and Sugiyam Y (2017) Analysis of Nonlinear Pharmacokinetics of a Highly Albumin-Bound Compound: Contribution of Albumin-Mediated Hepatic Uptake Mechanism. *J Pharmaceutical Sci* **106**:2704-2714.

Haapalinna A, Viitamaa T, MacDonald E, Savola JM, Tuomisto L, Virtanen R and Heinonen E (1997) Evaluation of the effects of a specific alpha 2-adrenoceptor antagonist, atipamezole, on alpha 1- and alpha 2-adrenoceptor subtype binding, brain neurochemistry and behavior in comparison. *Naunyn-Schmiedeberg's Arch Pharmacol* **5**:570-582.

Han YH, Kato Y, and Sugiyama Y (1999) Nonlinear disposition kinetics of a novel antifolate, MX-68, in rats. *J Pharmacol Exp Ther* **291**:204-212.

Hawes EM (1998) N-glucuronidation, a common pathway in human metabolism of drugs with a tertiary amine group. *Drug Metab Dispos* **26**:830-837.

Houston JB (1994) Utility of *in vitro* drug metabolism data in predicting *in vivo*

metabolic clearance. *Biochem Pharmacol* **47**:1469-1479.

Huang SM and Rowland M (2012) The role of physiologically based pharmacokinetic modeling in regulatory review. *Clin Pharmacol Ther* **91**:542-549.

Jamei M, Dickinson GL, and Rostami-Hodjegan A (2009) A framework for assessing interindividual variability in pharmacokinetics using virtual human populations and integrating general knowledge of physical chemistry, biology, anatomy, physiology and genetics: a tale of 'bottom-up' vs 'top-down' recognition of covariates. *Drug Metab Pharmacokinet* **24**:53-75.

Jones HM, Chen Y, Gibson C, Heimbach T, Parrott N, Peters SA, Snoeys J, Upreti VV, Zheng M, and Hall SD (2015) Physiologically based pharmacokinetic modeling in drug discovery and development: a pharmaceutical industry perspective. *Clin Pharmacol Ther* **97**:247-262.

Kaivosaari S, Finel M, and Koskinen M (2011) N-glucuronidation of drugs and other xenobiotics by human and animal UDP-glucuronosyltransferases. *Xenobiotica* **41**: 652-669.

Karhuvaara S, Kallio A, Scheinin M, Anttila M, Salonen JS and Scheinin H (1990) Pharmacological effects and pharmacokinetics of atipamezole, a novel á2-adrenoceptor antagonist - a randomized, double-blind cross-over study in healthy male volunteers. *Br J Clin Pharmacol* **30**:97-106.

Kaivosaari S, Toivonen P, Aitio O, Sipila J, Koskinen M, Salonen JS and Finel M (2008) Regio- and stereospecific N-glucuronidation of medetomidine: the differences between UDP glucuronosyltransferase (UGT) 1A4 and UGT2B10 account for the complex kinetics of human liver microsomes. *Drug Metab Dispos* **36**:1529-1537.

Li M, Zhao P, Pan Y, and Wagner C (2018) Predictive Performance of Physiologically Based Pharmacokinetic Models for the Effect of Food on Oral Drug Absorption: Current Status. *CPT Pharmacometrics Syst Pharmacol* **7**: 82-89.

Li Z, Gao Y, Yang C, Qiu X, Zhang T, Zhang W, Su R, Zhuang X (2018). *In vitro* metabolism of atipamezole in different species of liver microsomes and cytochrome P450 enzymes by high-resolution mass spectrometry. *Chin J Pharmacol Toxicol*, **32**: 946-952.

Li Z, Zhang Y, GaoY, XiangY, Zhang W, Lu C and Zhuang XM (2019) Atipamezole is a promising non-discriminative inhibitor against pan- CYP450 including

diclofenac 4′-hydroxylation: A comparison with ABT for drug ADME optimization and mechanism study. *Eur J Pharm Sci* **130**: 156-165.

Liu F, Zhuang XM, Yang C, Li, Xiong S, Zhang ZW, Li J, Lu C and Zhang ZQ (2014) Characterization of preclinical *in vitro* and *in vivo* ADME properties and prediction of human PK using a physiologically based pharmacokinetic model for YQA-14, a new dopamine D3 receptor antagonist candidate for treatment of drug addiction. *Biopharm Drug Dispos* **35**:296-307.

Lu C, Li P, Gallegos R, Uttamsingh V, Xia CQ, Miwa GT, Balani SK and Gan LS (2006) Comparison of Intrinsic Clearance in Liver Microsomes and Hepatocytes from Rats and Humans: Evaluation of Free Fraction and Uptake in Hepatocytes. *Drug Metab Dispos* **34**:1600-1605.

Ludden TM (1991) Nonlinear pharmacokinetics: clinical implications. *Clin Pharmacokinet* **20**:429-446.

Miller NA, Reddy MB, Heikkinen AT, Lukacova V and Parrott N (2019) Physiologically Based Pharmacokinetic Modeling for First In Human Predictions: An Updated Model Building Strategy Illustrated with Challenging Industry Case Studies. *Clin Pharmacokinet* **58**:727-746.

Nath A and Atikins WM (2006) A Theoretical Validation of the Substrate Depletion Approach to Determining Kinetic Parameters. *Drug Metab Dispos* **34**:1433-1435.

Obach RS and Reed-Hagen AE (2002) Measurement of Michaelis constants for cytochrome P450-mediated biotransformation reactions using substrate depletion approach. *Drug Metab Dispos* **30**:831-837.

Pertovaara A, Haapalinna A, Sirviö J and Virtanen R (2005) Pharmacological Properties, Central Nervous System Effects, and Potential Therapeutic Applications of Atipamezole, a Selective á2-Adrenoceptor Antagonist. *CNS Drug Rev* **3**:273-288.

Pertovaara A, Linnankoski I, Artchakov D, Rämä P and Carlson S (2004) Apotential aphrodisiac for female macaques. *Pharmacol Biochem Behav* **79**:137-141.

Pitkänen A, Narkilahti S, Bezvenyuk Z, Haapalinna A and Nissinen J (2004) Atipamezole, an á2-adrenoceptor antagonist, has disease modifying effects on epileptogenesis in rats. *Epilepsy Re*s **61**:119-140.

Puurunen K, Jolkkonen J, Sirviö J, Haapalinna A and Sivenius J (2001) An α_2-adrenergic antagonist, atipamezole, facilitates behavioral recovery after focal cerebral ischemia in rats. *Neuropharmacol* **40**:597-606.

Rowland M, Peck C, and Tucker G (2011) Physiologically-based pharmacokinetics in drug development and regulatory science. *Annu Rev Pharmacol Toxicol* **51**:45-73.

Shebley M, Sandhu P, Emami Riedmaier A, Jamei M, Narayanan R, Patel A, Peters SA, Reddy VP, Zheng M and de Zwart L (2018) Physiologically based pharmacokinetic model qualification and reporting procedures for regulatory submissions: a consortium perspective. *Clin Pharmacol Ther* **104**:88-110.

Smith DA, van Waterschoot RAB, Parrott NJ, Olivares-Morales A, Lavé T, and Rowland M (2018) Importance of target-mediated drug disposition for small molecules. *Drug Disco Today* **23**:2023-2030.

Tachibana T, Kato M and Sugiyama Y (2012) Prediction of nonlinear intestinal absorption of CYP3A4 and P-glycoprotein substrates from their *in vitro* K_m values. *Pharm Res* **29**:651-668.

Takeuchi T, Tagawa Y, Hagihara K, Maeshiba Y, Yamashita K, Tsukuda R, and Yoshimura Y (2001) Nonlinear pharmacokinetics of TAK-044, a new endothelin antagonist, in rats. *Biopharm Drug Dispos* **22**:221-230.

Tang H and Mayersohn M (2006) A global examination of allometric scaling for predicting human drug clearance and the prediction of large vertical allometry. *J pharm sci* **95**:1783-1799.

Viitamaa T, Haapalinna A and Heinonen E (1995) The effect of the á2-adrenoceptor antagonist, atipamezole, on the sexual behavior of sexually low-active male rats. *Behav Pharmacol* **6**:634-635.

Wu F, Gaohua L and Zhao P (2014) Predicting nonlinear pharmacokinetics of omeprazole enantiomers and racemic drug using physiologically based pharmacokinetic modeling and simulation: application to predict drug/genetic interactions. *Pharm Res* **31**:1919-1929.

Yang QJ, Si L, Tang H, Sveigaard HH, Chow EC and Pang KS (2015) PBPK modeling to unravel nonlinear pharmacokinetics of verapamil to estimate the fractional clearance for verapamil N-demethylation in the recirculating rat liver preparation. *Drug Metab Dispos* **43**:631-645.

Zhuang XM and Lu C (2016) PBPK modeling and simulation in drug research and development. *Acta Pharmaceutica Sinica B* **6:**430-440.

Footnotes

Dr. Zhuang was supported by National Science & Technology Major Special Project on

Major New Drug Innovation, China [2018ZX09711003-006] and [AWS16J016]. Dr. Zhang was supported by National Science & Technology Major Special Project on Major New Drug Innovation, China [2018ZX09721003-001-005].

FIGURE LEGENDS

Fig. 1. Chemical structure of atipamezole.

Fig. 2. Work flow scheme of the atipamezole PBPK model construction, verification and prediction.

Fig. 3. *In vitro* metabolic stability of atipamezole.
Amounts of atipamezole remaining after incubation in pooled RLM (A) or HLM (B) at various times are shown as a percentage compared to the amount at time zero. The values represent as means ± S.D. (n=3).

Fig. 4. Measurement of Michaelis constant of atipamezole for metabolizing enzyme mediated biotransformation reaction in RLM and HLM.
A: Plots of *in vitro* depletion rate constants versus atipamezole concentration- "*in vitro* $t_{1/2}$ method" was used to yield K_m value in RLM. B: Enzyme kinetic profiles of atipamezole-glucuronide formation in HLM (rates of atipamezole-G formation are shown as transferred amounts of atipamezole-glucuronide based on parent disappearance as described in the method section). The selected *in vitro* concentrations cover the *in vivo* plasma concentrations in rats from linear PK to nonlinear PK. The values represent as means ± S.D. (n=3).

Fig. 5. Plasma atipamezole concentration versus time curves in rats after intravenous and intramuscular administration at different dosages.
Existences of nonlinear pharmacokinetics (A and B) are manifested by the dose-normalized (C and D) plasma drug concentration versus time profiles in both routes.

Fig. 6. Observed and predicted concentration-time profiles of atipamezole in rats after *i.v.* 0.3mg/kg.
Black open circles represent concentrations obtained in rats; black line represents the simulated concentration-time profiles with a physiologically based pharmacokinetic model using measured K_p; gray dashed line represents the simulated concentration-time profiles with a physiologically based pharmacokinetic model using predicted K_p generated from Lukacova method.

Fig. 7. Observed and predicted concentration-time profiles of atipamezole doses in rats (A) single 0.3 mg/kg *i.v.* (B) single 0.9 mg/kg *i.v.* (C) single 3 mg/kg *i.v.* (D) single 0.1 mg/kg *i.m.* (E) single 1 mg/kg *i.m.* (F) single 3 mg/kg *i.m.*
The solid black line represents the simulated concentration-time profiles of atipamezole, the points on the graph are the observed mean concentrations.

Fig. 8. Observed and predicted concentration-time profiles of (A) single 10 mg i.v. dose of atipamezole (B) single 30 mg i.v. dose of atipamezole (C) single 100 mg i.v.

dose of atipamezole in human.
The solid black line represents the simulated concentration-time profiles of atipamezole, the points on the graph are the observed mean concentrations.

Fig. 9. Predicted dose dependent exposure of atipamezole in Chinese.
(A) predicted concentration-time profile of atipamezole in plasma; (B) predicted concentration-time profile of atipamezole in brain.

DMD Fast Forward. Published on November 7, 2019 as DOI: 10.1124/dmd.119.089151
This article has not been copyedited and formatted. The final version may differ from this version.

Tables

Table 1 Physicochemical and ADME parameters of atipamezole used for PBPK models

Parameter	Value	Source
Molecular weight (g/mol)	212.3	GastroPlusTM^{TM} 9.6
p*K*a	7.08, 13.33	GastroPlusTM^{TM} 9.6
LogD at pH 7.4	3.1	GastroPlusTM^{TM} 9.6
Solubility at pH 8.98 (mg/ml)	0.17	GastroPlusTM^{TM} 9.6
R_{bp} in rat	1.07	Measured *in this study*
R_{bp} in human	0.77	Measured *in this study*
$f_{u,p}$ and $f_{u,mic}$ of rat	0.085, 0.38	Measured *in this study*
$f_{u,p}$ and $f_{u,mic}$ of human	0.067, 0.59	Measured *in this study*
K_m of rat, human metabolizing enzyme (μM)	1.70 (361ng/ml), 2.89 (614 ng/ml)	Measured *in this study*
V_{max} of rat, human metabolizing enzyme (nmol/min/mg (protein))	0.131, 1.07	Measured *in this study*
Population information	Caucasia, Males, 23-year-old, height 182, weight 73kg	Karhuvaara et al., 1990

Table 2 Tissue partitions (K_p) of atipamezole measured in rats and the extrapolated values in human PBPK modeling

Tissue	Measured K_p of rat (n=6)	f_{ut} (%) (n=3)	K_{puu} of rat (n=6)	Transformed K_p of human[a]	Predicted K_p of rat[b]
brain	4.4±0.6	3.7±0.2	1.9±0.5	3.5	13.77*
adipose	0.4±0.2	2.9±0.2	0.1±0.06	0.3	7.79*
spleen	2.9±0.6	3.7±0.03	1.4±0.5	2.3	4.12
heart	1.3±0.6	2.4±0.1	0.4±0.03	1.0	3.77*
lung	6.1±2.3	1.8±0.08	1.3±0.4	4.8	6.07
muscle	0.6±0.3	2.9±0.5	0.2±0.08	0.5	2.65*
kidney	11.4±4.4	1.0±0.05	1.4±0.5	9.0	6.62
liver	23±8.9	0.02±0.01	0.06±0.02	18.1	6.34*
reproductive organ	4.7±4	2.7±0.1	1.5±0.6	3.7	6.63

a: K_p in human is transformed from rat K_p according to $K_{p\ uu\ of\ human} = K_{p\ uu\ of\ rat,}$ under the assumption that f_{ut} is identical between human and rat, namely, human K_p = rat K_p× (rat $C_{plasma,\ u}$/human $C_{plasma,\ u}$).

b: Predicted K_p in rat is obtained using Lukacova tissue-plasma partition method.

*: represents the ratio of predicted K_p of measured K_p is beyond 2-fold deviation.

Table 3 *In vitro* hepatic clearance atipamezole in liver microsomes of rats and humans in the presence of NADPH and UDPGA for metabolizing enzyme identification (n=3)

Metabolizing	HLM			RLM		
Enzyme	$t_{1/2}$ (min)	Cl_{int}(ml/min/kg)	Cl_h(ml/min/kg)	$t_{1/2}$ (min)	Cl_{int}(ml/min/kg)	Cl_h(ml/min/kg)
NADPH	93.5±33.8**	19.5±6.7**	9.7±1.8**	34.1±10.1	79.8±22.6	31.9±3.9
UDPGA	5.4±0.1	295.9±5.4	19.4±0.02	/	/	/
NADPH+UDPGA	5.4±0.2	295.2±9.9	19.3±0.04	33.4±2.0	75.0±4.8	31.7±0.8

The values represent as means ± S.D. (n=3).
*$p<0.05$ and **$p<0.01$ compared to NADPH+ UDPGA group.

DMD Fast Forward. Published on November 7, 2019 as DOI: 10.1124/dmd.119.089151
This article has not been copyedited and formatted. The final version may differ from this version.

Table 4 Unbound fraction of atipamezole in rat and human plasma at the relevant concentrations *in vivo*

Conc. (μM)	Rat	Human
0.3	0.071±0.008	0.068±0.016
1	0.095±0.005	0.060±0.006
3	0.090±0.005	0.073±0.004

The values represent as means ± S.D. (n=3).

Table 5 Pharmacokinetic parameters of atipamezole in rats after intravenous and intramuscular administration determined by noncompartmental analyses

Parameter	unit	intravenous administration			intramuscular administration		
		0.3mg/kg	0.9mg/kg	3mg/kg	0.1mg/kg	1mg/kg	3mg/kg
$t_{1/2}$	h	0.7±0.2	0.8±0.1	1.2±0.1	1±0.1	1±0.1	1.2±0.1
$AUC_{(0-t)}$	h×ng/ml	125.8±15.4	490.4±52.6	3776.3±785.7	43.6±14	542.8±80	3281.3±636.7
$AUC_{(0-\infty)}$	h×ng/ml	127.5±16.2	493.2±51.2	3780.8±779.9	44.9±13.9	543.8±80	3284.1±638
V	ml/kg	1624.3±162.5	1931.1±257.8	1497.3±161			
CL	ml/min/kg	39.96±5.83	30.73±3.07	13.96±3.64			
AUC/Dose	$\times 10^{-6}$h×kg/ml	419.3±51.4	544.8±58.5	1258.8±261.9**	449.45	543.79	1094.78**
T_{max}	h				0.19±0.08	0.13±0.09	0.46±0.27
C_{max}	ng/ml				49.8±13.9	553.2±75.1	1283.2±354.5
C_{max} /Dose	$\times 10^{-6}$kg/ml				497.83	553.17	427.72

The values represent as means ± S.D. (n=6).
*p<0.05 and **p<0.01 compared to low dose group.

DMD Fast Forward. Published on November 7, 2019 as DOI: 10.1124/dmd.119.089151
This article has not been copyedited and formatted. The final version may differ from this version.

Table 6 Predicted and observed pharmacokinetic parameters in rat and human receiving a single dose of atipamezole

Species	Route and dose	$AUC_{ped(0\text{-}inf)}$ h·ng/ml	$AUC_{obs(0\text{-}inf)}$ h·ng/ml	$AUC_{pre/obs}$ Fold error (FE)
rat	*i.v.* dose (mg/kg)			
	0.3	148.0	122.2	1.21
	0.9	592.8	479.2	1.24
	3	3931.0	3732.1	1.05
	i.m. dose (mg/kg)			
	0.1	52.5	46.1	1.14
	1	641.4	547.3	1.18
	3	2806.3	3289.0	0.85
human	*i.v.* dose (mg/person)			
	10	182.0	104.3	1.74
	30	566.9	370.2	1.53
	100	1893.5	1354.6	1.40

DMD Fast Forward. Published on November 7, 2019 as DOI: 10.1124/dmd.119.089151
This article has not been copyedited and formatted. The final version may differ from this version.

Table 7 Predicted and observed brain AUC of atipamezole in rat and human receiving a single *i.m.* of atipamezole

Species	dose	$AUC_{ped(0\text{-}inf)}$ h·ng/ml	$AUC_{obs(0\text{-}inf)}$ h·ng/ml
rat	0.3mg/kg	650	703
	1mg/kg	2500	2553
	3mg/kg	11500	16790
Human	10mg	600	
	30mg	2300	
	100mg	7400	

Fig. 1

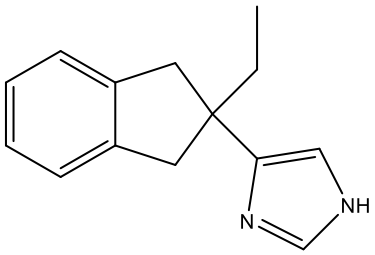

Fig. 2

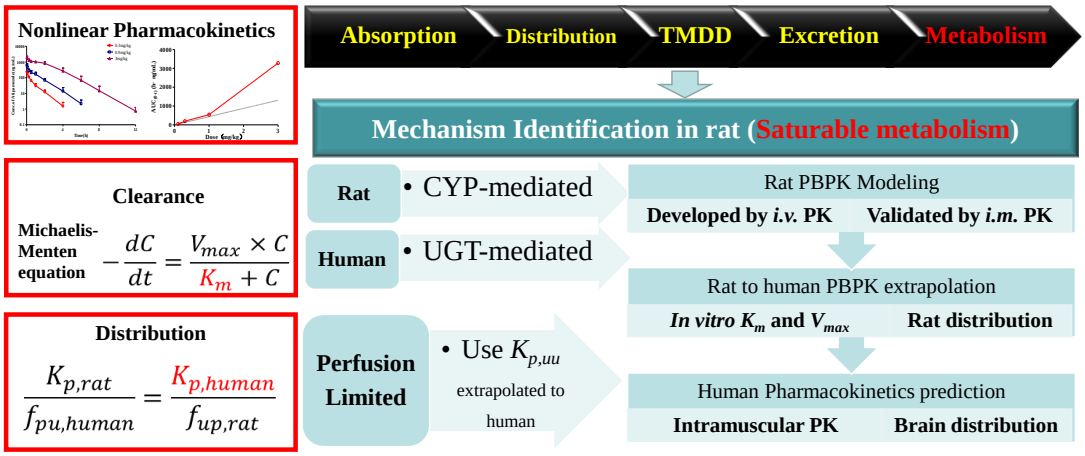

Fig. 3.

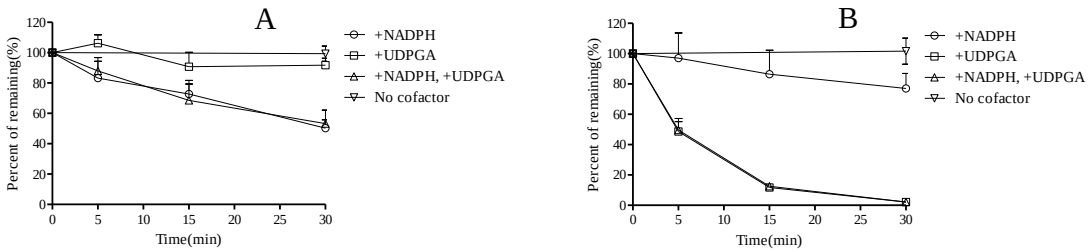

Fig. 4.

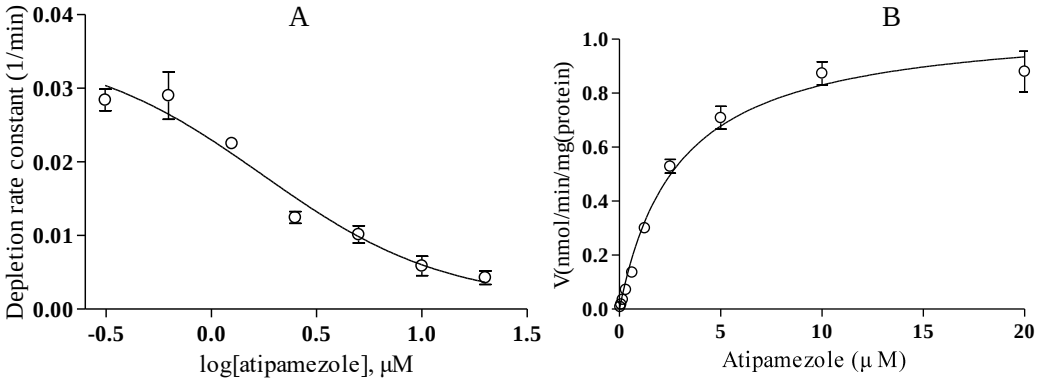

DMD Fast Forward. Published on November 7, 2019 as DOI: 10.1124/dmd.119.089151
This article has not been copyedited and formatted. The final version may differ from this version.

Fig. 5.

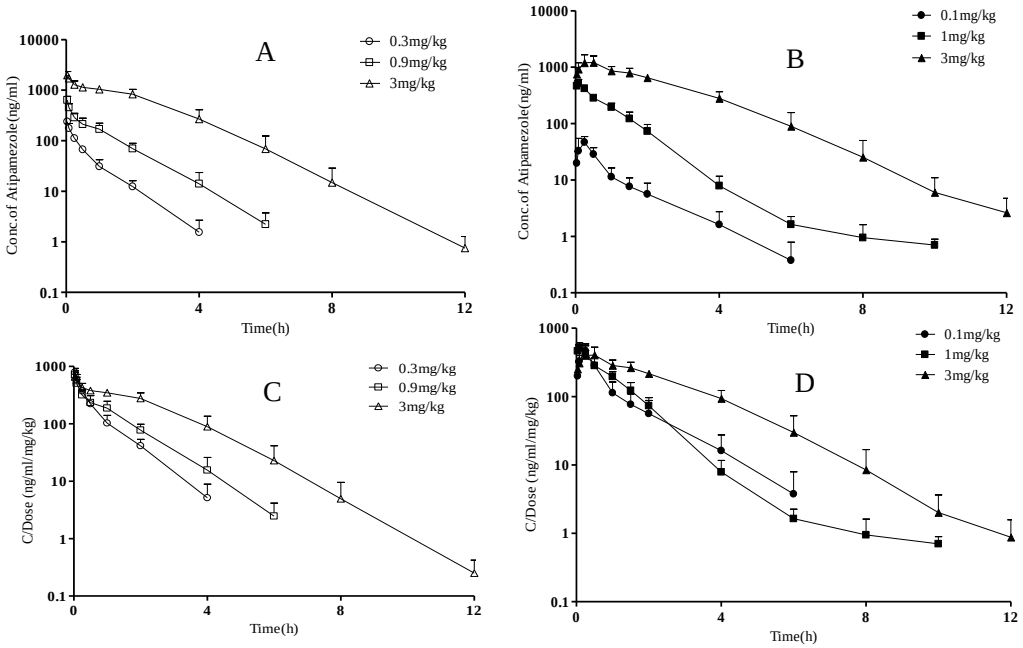

DMD Fast Forward. Published on November 7, 2019 as DOI: 10.1124/dmd.119.089151
This article has not been copyedited and formatted. The final version may differ from this version.

Fig. 6.

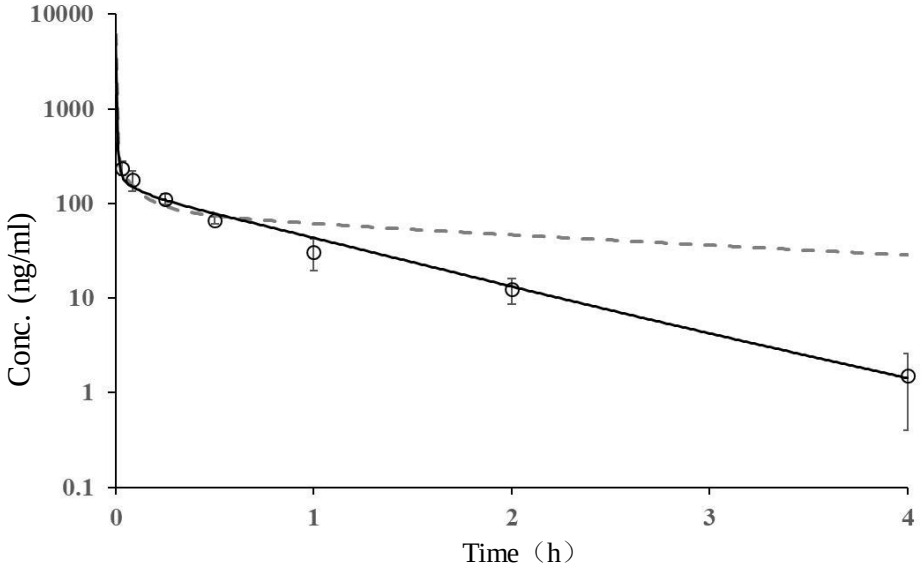

DMD Fast Forward. Published on November 7, 2019 as DOI: 10.1124/dmd.119.089151
This article has not been copyedited and formatted. The final version may differ from this version.

Fig. 7.

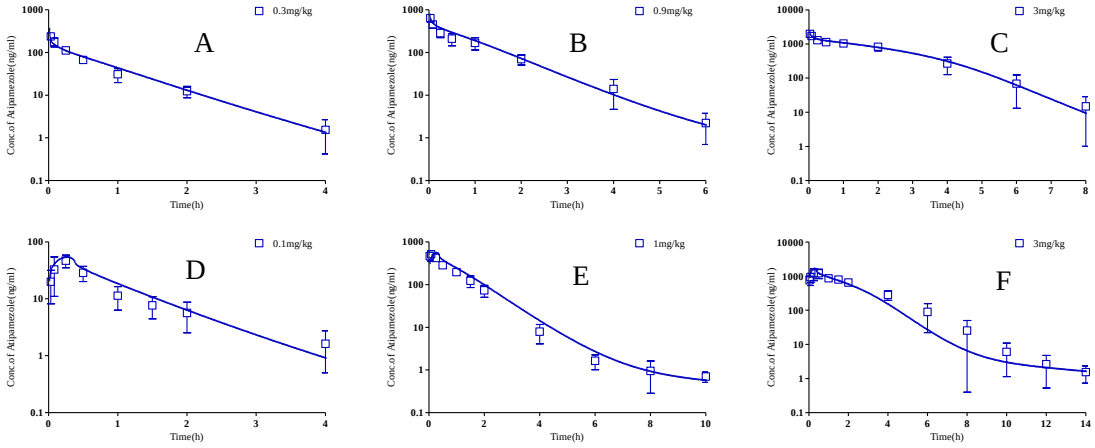

Fig. 8.

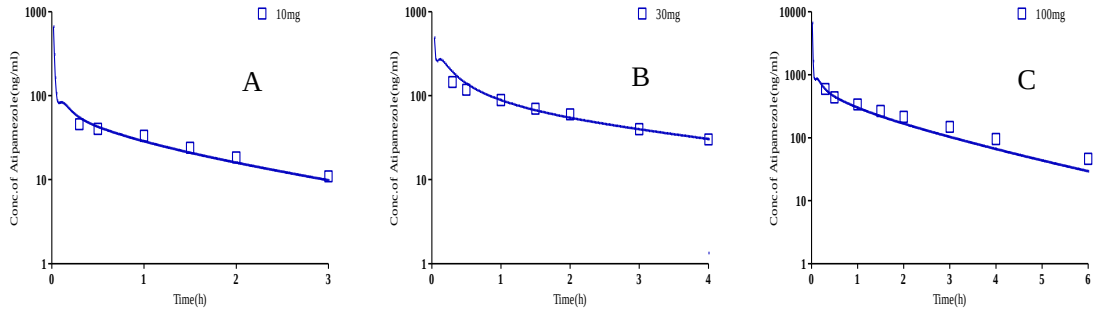

DMD Fast Forward. Published on November 7, 2019 as DOI: 10.1124/dmd.119.089151
This article has not been copyedited and formatted. The final version may differ from this version.

Fig. 9.